Constrained Predictive Control of Three-PhaseBuck Rectifiers

László Richárd Neukirchner[1], Attila Magyar[1], Attila Fodor[1], Nimród Dénes Kutasi[2], András Kelemen[2]

[1] University of Pannonia, Department of Information Technology, Egyetem u. 10, 8200 Veszprém, Hungary, e-mails: neukirchner.laszlo@virt.uni-pannon.hu, magyar.attila@virt.uni-pannon.hu, foa@almos.uni-pannon.hu

[2] Sapientia Hungarian University of Transylvania, Department of Electrical Engineering, Corunca 540485, Romania, e-mail: kutasi@ms.sapientia.ro, kandras@ms.sapientia.ro

Abstract: In this paper, constrained optimal control of a current source rectifier (CSR) is presented, based on a mathematical model developed in Park's frame. To comply with the system constraints an explicit model-based predictive controller was established. To simplify the control design, and avoid linearization, a disjointed model was utilised due to the significant time constant differences between the AC and DC side dynamics. As a result, active damping was used on the AC side, and explicit Model Predictive Control (MPC) on the DC side, avoiding non-linear dynamics. The results are compared by simulation with the performance of a state feedback control.

Keywords: model predictive control; current source rectifier; space vector modulation; modeling; constrained control

1 Introduction

Current source rectifiers (CSR) are widely used in front-end power electronic converter for the uncontrollable or controllable DC-bus in industrial and commercial applications. They have maintained their position through many applications, with uses such as medium-voltage high-power drives [1], [2] STATCOMs [3] and renewable systems [4], [5]. They have a plain and reliable circuit structure, which makes them attractive for simple control design. The CSRs are traditionally controlled by classic cascaded linear control loops such as PI controllers. These simple control applications are suitable for induction motor control [6], and other electromechanical actuators [7], and unusual topologies [8]. Also, worth mentioning is self-tuning variants of PI controllers [9]. In the past, the modulation methods used were trapezoidal pulse width modulation techniques

(TPWM), or application of pulse patterns calculated offline for selective harmonic elimination (SHE). More recently, current space vector modulation (SVM) has been used for the synthesis of the transistor control signals [10]. Even so, AC-side harmonic elimination could still be an issue at lower switching frequencies where LCL filtering would be advised [11]. In order to keep switching frequencies low and to minimize switching losses, new topologies and hybrid modulations are used, mixing TPWM and SHE depending on the grid frequency [12].

In terms of the amplitude of the grid and DC-link voltages, CSRs exhibit a step-down conversion. When used as DC voltage source, the rectifier can output a lower DC voltage without the need of a grid-side transformer, as is usually employed in voltage source rectifiers (VSR). Because of their current source behaviour, CSRs can be easily paralleled and provide inherent short-circuit protection, representing an excellent potential in DC power supply applications [13], [14].

There are several control strategies in addition to classical PI control for applications in this domain. Self-adapting control methods are on the rise with more sophisticated algorithms in the field of fuzzy logic [15]. They are capable of handling increasingly more complicated models and systems with high dynamics and accuracy [16], [17], and even without establishing and validating classical state-space models [18]. The other filed is the sliding mode control, which can achieve good dynamic performance and handle non-linearity. Still, they might also introduce chattering, which can be very undesirable when applied to real-life systems like in [19] and [20].

In the linear domain implicit model predictive control (IMPC or just MPC) is a fair solution due its; effectiveness in power electronics, configurable cost function and such scalable nature [21], [22]. In this field also finite-state solutions are present which can be considered also predictive control, where the modulation scheme's defined states serve as optimization potential [23], [24]. As a further step adaptive application was established to tackle parameter estimation problems for better performance [25]

Recently, beside implicit, finite-state, and adaptive predictive control, explicit model predictive control has emerged in the field of power electronics [26]. Establishing the MPC cost function can range widely depending on the expected dynamics, degree of noise cancellation, and model complexity. Additionally, the current limitation can also be implemented introducing constraints in the modulation algorithm.

In [27] the validity of an MPC-based, digital pulse width modulation control strategy for single-phase voltage source rectifiers is discussed, further confirming the validity of this method in control systems.

1.1 New Contributions

In this paper a model predictive control method is developed for a classical current source buck-type rectifier (CSR). The contribution of the paper is to show how to design EMPC on a model of a CSR which has a complex model due to bilinearity. To overcome the burden of bilinearity a simple solution is shown which enables handling the model parts as linear disjointed systems of their own.

The structure of the paper is as follows. In Section 2 the topology is presented, followed by the mathematical model derived in the synchronous rotating coordinate frame. Next, the control structure is presented, followed by the detailed description of the DC-side Explicit Model Predictive Control (EMPC) and by the presentation of the AC-side active damping. In the fourth section, the current space vector modulation scheme is shown, with optimized switching pattern to reduce the switching frequency. Lastly, the simulation results are presented and the performance of the proposed control structure is compared with the performance of a state feedback controller, before the conclusions are finally drawn.

2 Mathematical Modeling of the CSR

The structure of the classical three phase buck-type current source rectifier (CSR) is presented in Fig. 1. In continuous current mode, the differential equations corresponding to the CRS's inductor currents and capacitor voltages are the following:

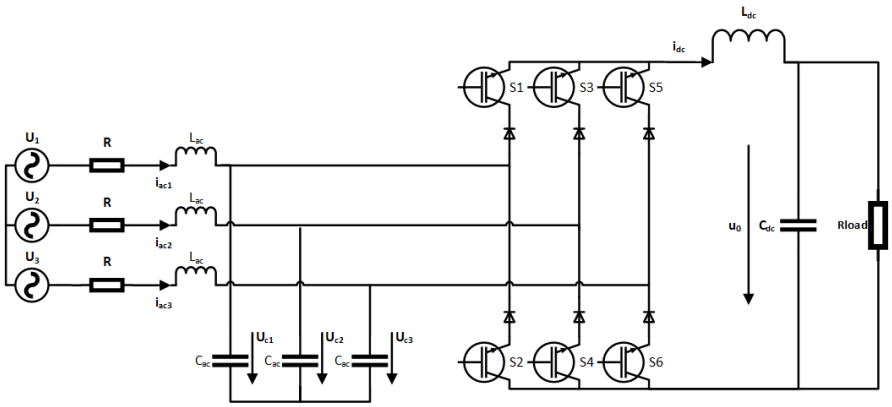

Figure 1
Circuit diagram of the three-phase buck-type rectifier with insulated gate bipolar transistors (IGBTs)

$$L_{ac}\dot{\imath_{ac_p}} = u_p - u_{c_p} - Ri_{ac_p} \tag{1}$$

$$
\begin{aligned}
C_{ac}\dot{u_{c_p}} &= i_{ac_p} - \delta_p i_{dc} \\
L_{dc}\dot{\imath_{dc}} &= \left(\sum_{p=1}^{3} \delta_p \, u_{c_p}\right) - u_0 \\
C_{dc}\dot{u_0} &= i_{dc} - \frac{u_0}{R_{load}}
\end{aligned}
$$

where $p \in \{1,2,3\}$ is the index of three phases and δ_p describes the conduction state of the rectifier leg p (2).

$$
\delta_p = \begin{cases} 1 \; if \; the \; upper \; transitor \; is \; ON \\ -1 \; if \; the \; lower \; transistor \; is \; ON \\ 0 \; if \; both \; are \; ON \; or \; OFF \end{cases} \tag{2}
$$

Using the components in the stationary frame of the space phasors of the three-phase quantities, from (1) it results:

$$
\begin{aligned}
L_{ac}\dot{\imath_{ac_\alpha}} &= u_\alpha - u_{c_\alpha} - R i_{ac_\alpha} \\
L_{ac}\dot{\imath_{ac_\beta}} &= u_\beta - u_{c_\beta} - R i_{ac_\beta} \\
C_{ac}\dot{u_{c_\alpha}} &= i_{ac_\alpha} - \delta_\alpha i_{dc} \\
C_{ac}\dot{u_{c_\beta}} &= i_{ac_\beta} - \delta_\beta i_{qc} \\
L_{dc}\dot{\imath_{dc}} &= 1.5\left(\delta_\alpha u_{c_\alpha} + \delta_\beta u_{c_\beta}\right) - u_0 \\
C_{dc}\dot{u_0} &= i_{dc} - \frac{u_0}{R_{load}}
\end{aligned} \tag{3}
$$

Equation (3) is transformed to the synchronous reference frame rotating with the u_{c_d} capacitor voltage space vector. The resulting mathematical model is thus:

$$
\begin{aligned}
L_{ac}\dot{\imath_{ac_d}} &= u_d - u_{c_d} - R\mathrm{i}_{ac_d} + \omega_s L_{ac}\mathrm{i}_{ac_q} \\
L_{ac}\dot{\imath_{ac_q}} &= u_q - u_{c_q} - R\mathrm{i}_{ac_q} - \omega_s L_{ac}\mathrm{i}_{ac_d} \\
C_{ac}\dot{u_{c_d}} &= i_{ac_d} - \delta_d i_{dc} + \omega_s C_{ac} u_{c_q} \\
C_{ac}\dot{u_{c_q}} &= i_{ac_q} - \delta_q i_{dc} - \omega_s C_{ac} u_{c_d} \\
L_{dc}\dot{\imath_{dc}} &= 1.5\left(\delta_d u_{c_d} + \delta_q u_{c_q}\right) - u_0 \\
C_{dc}\dot{u_0} &= i_{dc} - \frac{u_0}{R_{load}}
\end{aligned} \tag{4}
$$

where ω_s represents the network voltage vector's angular velocity.

2.1 Model Simplification

Notice, that the sixth-order ODE model (4) is bilinear in its states and inputs because of the product terms ($\delta_d i_{dc}$ for example). As such, using design methods for linear systems is not straightforward. The high complexity given by the system's order is another problem to tackle. For designing classic MPC, linear, low-order equation systems are favorable. Hence

simplification of the model would bring noteworthy benefits, making the MPC design more straightforward, when a linear system resulted.

Since the AC and DC side's time constants differ significantly (as in the AC: $\omega_{ac} = \frac{1}{\sqrt{L_{ac}C_{ac}}} \cong 5.7 \cdot 10^3 [rad/s]$, and on the DC:$\omega_{dc} = \frac{1}{\sqrt{L_{dc}C_{dc}}} \cong 2.8 \cdot 10^2 [rad/s]$, see Table 3. for reference). Thus, the differential equations can be separated into two sets, and the control of the AC and DC sides can be decoupled as described in [28]. The AC side model results as follows:

$$\begin{pmatrix} \dot{\imath}_{ac_d} \\ \dot{\imath}_{ac_q} \\ \dot{u}_{c_d} \\ \dot{u}_{c_q} \end{pmatrix} = \begin{pmatrix} -\frac{R}{L_{ac}} & \omega_s & -\frac{1}{L_{ac}} & 0 \\ -\omega_s & -\frac{R}{L_{ac}} & 0 & -\frac{1}{L_{ac}} \\ \frac{1}{C_{ac}} & 0 & 0 & \omega_s \\ 0 & \frac{1}{C_{ac}} & -\omega_s & 0 \end{pmatrix} \begin{pmatrix} i_{ac_d} \\ i_{ac_q} \\ u_{c_d} \\ u_{c_q} \end{pmatrix} + \begin{pmatrix} \frac{u_d}{L_{ac}} \\ \frac{u_q}{L_{ac}} \\ -\frac{\delta_d i_{dc}}{C_{ac}} \\ -\frac{\delta_q i_{dc}}{C_{ac}} \end{pmatrix}. \tag{5}$$

Looking at the state matrix it can be further stated that there are only weak couplings between the d and q components. This allows to handle them separately, and later to design separate control for each.

The equation system describing the DC side dynamics is the following:

$$\begin{pmatrix} \dot{\imath}_{dc} \\ \dot{u}_0 \end{pmatrix} = \begin{pmatrix} 0 & \frac{-1}{L_{dc}} \\ \frac{1}{C_{dc}} & \frac{-1}{R_{load}C_{dc}} \end{pmatrix} \begin{pmatrix} i_{dc} \\ u_0 \end{pmatrix} + \begin{pmatrix} \frac{1.5}{L_{dc}} \left(\delta_d u_{c_d} + \delta_q u_{c_q} \right) \\ 0 \end{pmatrix}. \tag{6}$$

It can be noticed that, with the AC and DC model separation, bilinearity disappears, since the binding coefficients are present only in the input ($\boldsymbol{u}$) of the DC state space model. Consequently, all equations are linear and with a considerably lower order, making control design much easier and allowing for the application of linear design methods. For the DC side dynamics, the linear time invariant differential equation system's matrices can be identified for predictive control design purposes:

$$\boldsymbol{x} = \begin{pmatrix} i_{dc} \\ u_0 \end{pmatrix}, \boldsymbol{u} = \left(\delta_d u_{c_d} + \delta_q u_{c_q} \right), \boldsymbol{y} = u_0,$$

$$\boldsymbol{A} = \begin{pmatrix} 0 & \frac{-1}{L_{dc}} \\ \frac{1}{C_{dc}} & \frac{-1}{R_{load}C_{dc}} \end{pmatrix}, \boldsymbol{B} = \begin{pmatrix} \frac{1.5}{L_{dc}} \\ 0 \end{pmatrix}, \boldsymbol{C} = (0 \quad 1). \tag{7}$$

where $\boldsymbol{x}$, $\boldsymbol{u}$and $\boldsymbol{y}$are the state, input and output vectors of the DC-side system, and $\boldsymbol{A}$, $\boldsymbol{B}$ and $\boldsymbol{C}$ are the state, input and output matrices.

The circuit parameters used for the implementation of the control structure based on this model are presented in Table 3.

3 The Control Structure

Relying on the possibility of separation of the AC-side and DC-side controllers, the control structure from Fig. 2 is proposed.

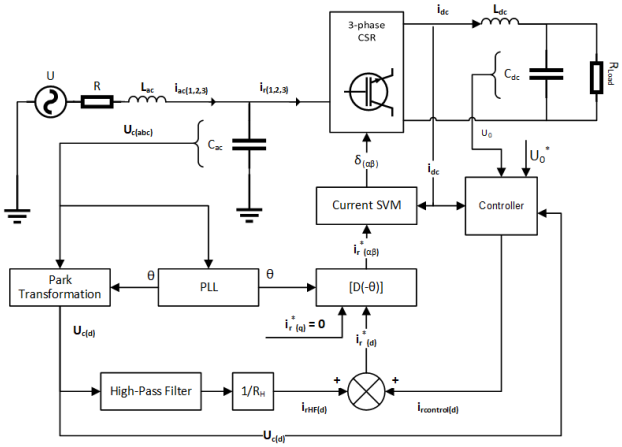

Figure 2

Block diagram of the control structure

The controllers operate in the synchronous frame of the AC filter capacitor voltages $u_{c_{(1,2,3)}}$, and the rectifier input currents $i_{r_{(1,2,3)}}$ are in phase with the capacitor voltages.

The current reference $i^*_{r(\alpha\beta)}$ supplied to the space vector modulation unit in the stationary frame, is obtained by coordinate transformation $[D(-\theta)]$ of the current reference (8) delivered by the current controllers in the synchronous frame.

$$\begin{cases} i^*_{r_d} = i_{rcontrol_d} + i_{rHF_d} \\ i^*_{r_q} = 0 \end{cases} \tag{8}$$

In (8), $i_{rcontrol_d}$ represents the output of the DC voltage controller, while i_{rHF_d} represents the damping current, proportional with the high frequency component of the filter capacitor voltage (the fundamental component of the capacitor voltage in the stationary frame becomes a DC component in the synchronous frame). The DC and AC side control units are explained in more detail in the following sections, and the performance of the control structure is evaluated.

3.1 DC-SideExplicit Model Predictive Control

Model predictive control (MPC) is an efficient and systematic method for solving complex multi-variable constrained optimal control problems [3]. The MPC control law is based on the "receding horizon formulation", where the model's assumed behavior is calculated for a number of N steps, where N stands for the

horizon's length. Only the first step of the computed optimal input is applied in each iteration. The remaining steps of the optimal control input are discarded and a new optimal control problem is solved at the next sample time. Using this approach, the receding horizon policy provides the controller with the desired feedback characteristics, although with high order systems the computational effort is considerably demanding since all the steps should be taken in to account on the specified horizon in every iteration. With Explicit MPC (EMPC), the discrete time constrained optimal control problem is reformulated as multi-parametric linear or quadratic programming. Using this approach, the problem of optimization can be solved offline, making it much more feasible from the perspective of the optimal control task. The optimum control law is a piecewise affine function of the states, and the resulting solution is stored in a pre-calculated lookup table. The parameter space, or the state-space is partitioned into critical regions. The real-time implementation consists in searching for the active critical region, where the measured state variables lie, and in applying the corresponding piecewise affine control law to achieve the desired dynamics.

In order to introduce the MPC implementation from this paper, let us consider a linear discrete time system (9) derived with the discretisation of system (6) with zero-order hold method, where control inputs are assumed piecewise constant over the simulation sample time $T_s = 1/f_s$:

$$\begin{aligned} \boldsymbol{x}(t+1) &= \boldsymbol{A}_d\boldsymbol{x}(t) + \boldsymbol{B}_d\boldsymbol{u}(t) \\ \boldsymbol{y}(t) &= \boldsymbol{C}_d\boldsymbol{x}(t) \end{aligned} \tag{9}$$

where $\boldsymbol{A}_d, \boldsymbol{B}_d, \boldsymbol{C}_d$ere the matrices of the discretised system derived from (7). With system (9) appears to be linear time invariant, MPC design can be followed. The following constraints have to be satisfied:

$$\boldsymbol{y}_{min} \le \boldsymbol{y}(t) \le \mathbf{y}_{max}, \boldsymbol{u}_{min} \le \boldsymbol{u}(t) \le \boldsymbol{u}_{max} \tag{10}$$

where $t > 0$, $\boldsymbol{x} \in R^n, \boldsymbol{u} \in R^m, \boldsymbol{y} \in R^p$. The MPC solves the following constrained optimization problem [23]:

$$\min_{U=\{\boldsymbol{u}_t,\dots,\boldsymbol{u}_t+N_u-1\}} J(\boldsymbol{u}, \boldsymbol{x}(t)) = \sum_{k=0}^{N_y-1} \left(\boldsymbol{x}_{t+N_y \vee t}^T Q_w \boldsymbol{x}_{t+N_y \vee t} + \boldsymbol{u}_{t+k}^T R_w \boldsymbol{u}_{t+k} \right) \tag{11}$$

subject to:

$$\begin{aligned} &\boldsymbol{x}_{min} \le \boldsymbol{x}_{t+k|t} \le \boldsymbol{x}_{max}, k = 1, \dots, N_c - 1 \\ &\boldsymbol{u}_{min} \le \boldsymbol{u}_{t+k|t} \le \boldsymbol{u}_{max}, k = 0,1, \dots, N_c - 1 \\ &\boldsymbol{x}_{t|t} = \boldsymbol{x}(t) \\ &\boldsymbol{x}_{t+k+1|t} = \boldsymbol{A}_d\boldsymbol{x}_{t+k|t} + \boldsymbol{B}_d\boldsymbol{u}_{t+k|u} \\ &\boldsymbol{y}_{t+k+1|t} = \boldsymbol{C}_d x_{t+k|t} \\ &\boldsymbol{u}_{t+k|t} = -K\boldsymbol{x}_{t+k|t} \end{aligned} \tag{12}$$

$k \geq 0$

This problem is solved at each time instant *t*, where $\boldsymbol{x}_{t+k|t}$ denotes the state vector predicted at time *t+k*, obtained by applying the input sequence $\boldsymbol{u}_{t|t\ldots}\boldsymbol{u}_{t+k-1|t}$ to model (15), starting from the state $\boldsymbol{x}_{t|t}$. Further, it is assumed that the weighting matrices Q_w and R_w, are symmetric positive semidefinite ($Q_w = Q_w^T \geq 0, R_w = R_W^T > 0$) and K is a feedback gain. Further, N_y, N_u, N_c, are the output, input and constraint horizons, respectively.

Using the model for predicting the future behavior of the system and with some appropriate substitution and variable manipulation, the problem (11), (12) can be transformed to the standard multi-parametric quadratic programming (mp-QP) form, as described in [29]:

$$V_z(\boldsymbol{x}) = \quad min \frac{1}{2} z^t H z \tag{13}$$

subject to:

$$Gz \quad \leq \quad W + S\boldsymbol{x}(t) \tag{14}$$

where the matrices H, G, W, S result directly from the coordinate transformations and variable manipulations. The solution of the mp-QP problem for each critical region has the form:

$$\boldsymbol{u}^* = \quad f_i \boldsymbol{x} + g_i \tag{15}$$

and the critical region is described by:

$$C_{reg_i} = \quad \{\boldsymbol{x} \in R^n \vee H_i \boldsymbol{x} \leq K_i\}. \tag{16}$$

Thus, the explicit MPC controller is completely characterized by the set of parameters:

$$\{f_i, g_i, H_i, K_i\}^{i=1\ldots N}. \tag{17}$$

In case of the discrete time system resulting from (7), for sampling time equal with the switching period $T_s = 50 \cdot 10^{-5}\, s$, the problem defined to be solved by MPC is the minimization of the quadratic cost function (11) for:

$$R_w = \begin{bmatrix} 1 & 0 \\ 0 & 1 \end{bmatrix}, Q_w = \begin{bmatrix} 10^{-6} & 0 \\ 0 & 10^{-6} \end{bmatrix}, \text{and } N_y = N_u = N_c = 2. \tag{18}$$

Since N_y, N_u, N_c take the same value, they will be substituted by N.

The constraints defined based on the rated power of the CSR $P_N = 2500\, W$, are:

$$\begin{aligned} 0 \leq \quad i_{dc} \quad &\leq 50A \\ 0 \leq \quad u_0 \quad &\leq 500V \end{aligned} \tag{19}$$

The state space partition resulting from this problem has 13 critical regions, which can be observed in Fig. 3.

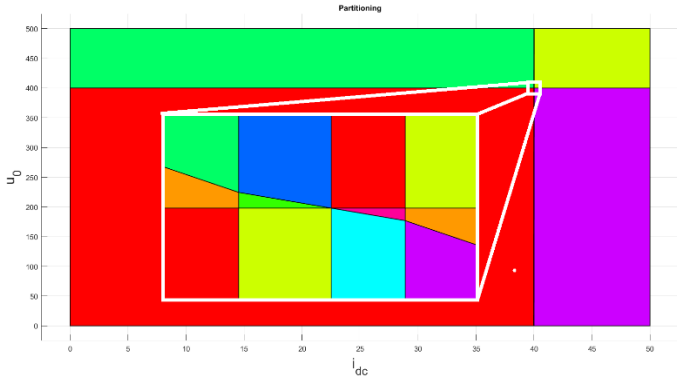

Figure 3
State space partitioning

From the basis of the discretized model (9), the given constraints, and horizon (19) the cost function (11) is established via the MPT toolbox [30] and used in the generated controller for the EMPC design [29], [31]. The controller is created as a compliable S-function in the Matlab/Simulink environment and its place in the control structure can be observed in Fig. 4 as the EMPC controller.

The output of the MPC controller is the control variable obtained via solving (12) $u_{MPC} = \left(\delta_d u_{c_d} + \delta_q u_{c_q}\right)$, from which the current reference can be calculated using (19). The quadrature component u_{c_q} is zero in the synchronous frame of the filter capacitor voltage.

$$i_{rMPC_d} = \frac{u_{MPC}}{u_{c_d}} \cdot i_{dc} \tag{20}$$

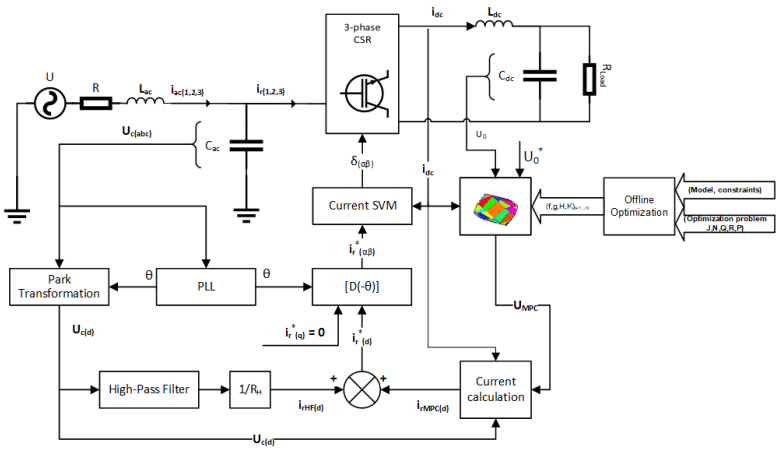

Figure 4

The control structure of the CSR, with MPC controller on the DC side

3.2 Active AC-Side Damping

The CSR requires a voltage supply on the AC side. Taking into consideration the inductive character of the mains, the presence of a three-phase capacitor tank at the input of the CSR is a must. The most convenient is to use three-phase LC filtering with inductors on the lines and star connected capacitors resembling those in Fig. 1, although the resonance phenomena between these components can still cause difficult problems. The simplest way to dampen the resonance on the AC side LC filter is to add a damping resistor across the capacitor [23]. Because these resistors result in high losses, active damping methods have been proposed, which emulate damping resistors by control. This makes the CSR bridge produce an additional high frequency current, equivalent to the presence of virtual damping resistors connected in parallel with the AC capacitors. The resonance of the AC side LC filter produces harmonics in the capacitor voltage with frequency close to $\omega_{ac} = \frac{1}{\sqrt{L_{ac}C_{ac}}}$, which appears as $\omega_{ac} - \omega_s$ component in u_{c_d}, where $\omega_s = 2\pi f$. The fundamental component of the capacitor voltage represents a DC component in the synchronous reference frame. Therefore, a high-pass filter (HPF) is applied to filter out this DC component, with the transfer function:

$$HPF(s) = \frac{s}{s + 0.1 * (\omega_{ac} - \omega_s)}. \tag{21}$$

A virtual damping resistance R_H has been defined for calculation of the damping current component i_{HPF} from the HF component of the capacitor voltage.

4 Space Vector Modulation Strategy

The chosen modulation strategy is developed in the "αβ" stationary reference frame. The structure requires simultaneous conduction of the upper and lower transistors of the bridge, since the current of the L_{dc}choke must not be interrupted. Additionally, the switching devices are considered as ideal.

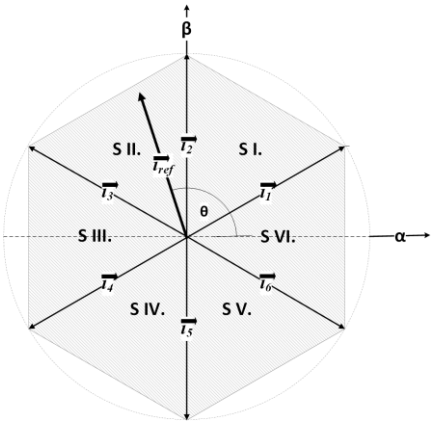

Figure 5

The fundamental input current vectors corresponding to the active switching states of the CSR

According to this, one of the upper and one of the lower switches must be closed at all times. This allows nine states, six of which are active. There are three "zero" vectors, corresponding to the switching states, when both devices of one of the bridge legs are in conduction, shown in Table 1.

Table 1

Switching states of the rectifier and the corresponding space phasors

Name	Switching State						Phase currents			Vector representation
	1	2	3	4	5	6	i_a	i_b	i_c	
$\vec{i_1}$	1	0	0	0	0	1	i_{dc}	0	-i_{dc}	$\left(2i_{dc}e^{\left(\frac{j\pi}{6}\right)}\right)/\sqrt{3}$
$\vec{i_2}$	0	0	1	0	0	1	0	i_{dc}	-i_{dc}	$\left(2i_{dc}e^{\left(\frac{j\pi}{2}\right)}\right)/\sqrt{3}$
$\vec{i_3}$	0	1	1	0	0	0	-i_{dc}	i_{dc}	0	$\left(2i_{dc}e^{\left(\frac{j5\pi}{6}\right)}\right)/\sqrt{3}$
$\vec{i_4}$	0	1	0	0	1	0	-i_{dc}	0	i_{dc}	$\left(2i_{dc}e^{\left(\frac{j7\pi}{6}\right)}\right)/\sqrt{3}$
$\vec{i_5}$	0	0	0	1	1	0	0	-i_{dc}	i_{dc}	$\left(2i_{dc}e^{\left(\frac{j3\pi}{2}\right)}\right)/\sqrt{3}$
$\vec{i_6}$	1	0	0	1	0	0	i_{dc}	-i_{dc}	0	$\left(2i_{dc}e^{\left(\frac{j11\pi}{6}\right)}\right)/\sqrt{3}$
$\vec{i_7}$	1	1	0	0	0	0	0	0	0	0
$\vec{i_8}$	0	0	1	1	0	0	0	0	0	0
$\vec{i_9}$	0	0	0	0	1	1	0	0	0	0

The neighboring space phasors can be formulated as:

$$\overrightarrow{i_n} = \frac{2}{\sqrt{3}} i_{dc} expj\left(\frac{n\pi}{3} - \frac{\pi}{6}\right)$$
$$\overrightarrow{i_{n+1}} = \frac{2}{\sqrt{3}} i_{dc} expj\left(\frac{n\pi}{3} + \frac{\pi}{6}\right) \quad (22)$$
$$n = 1,2,\dots 6$$

The reference current vector is sampled with fixed sampling period T_s. The sampled value of $\overrightarrow{i_{ref}}$ is synthesized as the time average of two neighbouring space phasors adjacent to the reference current:

$$T_n \overrightarrow{i_n} + T_{n+1} \overrightarrow{i_{n+1}} = T_s \overrightarrow{i_{ref}}. \quad (23)$$

T_n and T_{n+1} represent the individual durations of the switching states corresponding to the neighboring vectors. For example, in case of a current reference vector situated in the first sector, T1, T2 and T0 can be calculated using (24).

$$T_1 = T_s \frac{i_{ref_\alpha}}{i_{dc}}$$
$$T_2 = T_s \frac{\sqrt{3}}{2} \frac{1}{i_{dc}} \left(i_{ref_\beta} - \frac{1}{\sqrt{3}} i_{ref_\alpha}\right) \quad (24)$$
$$T_0 = T_s - T_n - T_{n-1} = T_{7,8,9}$$

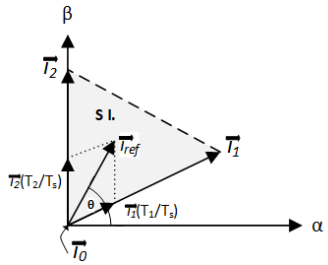

Figure 6
Synthesis of $\overrightarrow{i_{ref}}$ by $\vec{i}_1$, $\vec{i}_2$, and $\vec{i}_0$

The complex plane is naturally divided by the fundamental space vectors into six areas, named “sectors”.

$$\frac{\pi}{6} + \frac{(n-1)\pi}{3} \leq \theta_n \leq \frac{\pi}{6} + \frac{n\pi}{3} \quad (25)$$
$$n = 1,2,\dots 6$$

The non-zero space vectors are selected based on the phase angle θ between $\overrightarrow{i_{ref}}$ and the real axis. Table 2 presents an example of switching pattern in case of a current reference vector situated in Sector I.

Table 2
Representation of switching sequences for SECTOR I

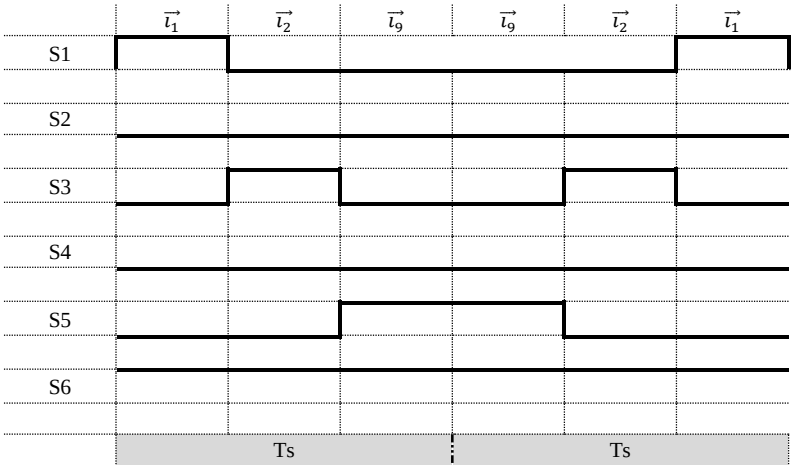

The switching scheme represented in Table 1 is aimed at reducing the number of commutations in a switching cycle, resulting in the reduction of the switching losses [32]. Additionally, the constraint (26) resulting from the available magnitudes of the current vectors, is applied to the current reference.

$$0 \leq \left|i_{ref}\right| \leq \frac{\sqrt{6} i_{dc}}{cos(\theta) + \sqrt{3} sin(\theta)} \tag{26}$$

5 Performance Evaluation

From the continuous AC (5), and DC (6) model equations described in Ch. 2, the controller is formulated form discretised system (9), and it is described via the cost function and control problem of (11), and (12) in Ch. 3. The evaluated model and control structure are shown on Fig. 4. In the following section said EMPC's computational requirements are evaluated, and the Matlab/Simulink simulation results are compared to a classic state feedback controller's dynamic performance.

5.1 Computational Effort

The binary search tree generated for the control problem presented in Fig. 7, and described in Ch. 3. The depth of the search tree is 5 and it has a total number of 29 nodes. It is utilized with the MPT toolbox [30], [31], [33] and it can be used for the computationally optimal real-time implementation of the proposed algorithm on low-cost hardware.

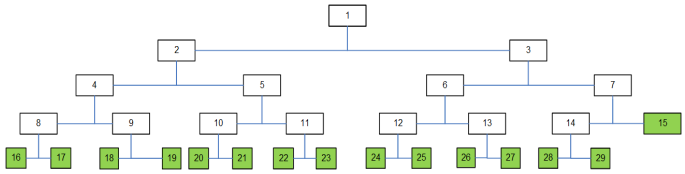

Figure 7

Binary search tree of the controller for a horizon of N=4. The leaf nodes are depicted with filled squares. The depth of the tree is 5.

The search for an active critical region starts from the first level and represents the evaluation in each adjacent node of an inequality of the form: $x \leq K$. Thus, in this case a maximum number of 4 inequalities have to be evaluated to reach the active critical region. Implementing the presented algorithm is straightforward on a DSP processor, for instance from the dsPIC33 family by Microchip. Using the *mac* (multiply and accumulate) instruction the inequality is evaluated for each node using 4 instructions, thus in 80 ns on a 50 MIPS processor (Fig. 8). The active critical region can be reached in a maximum of 400 ns. Compared to the typical sample rate of 10us in the case of a CSR, the real-time implementation on a DSP processor is possible.

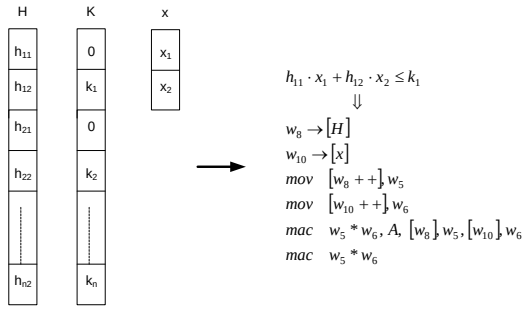

Figure 8

Data organization in the data memory of a single core DSP and the evaluation of a 2-dimensional inequality

5.2 Horizon Performance

With the cost function (11) employed using (18), changing the length of the horizon (*N*) affects the system's complexity illustrated by the partition in the state space shown in Fig. 3, and Fig. 11 presents the step response of the controlled system for different lengths of the horizon. It shows, that the response is not affected by the increase of the horizon above N=2, supporting the choice of this value for Matlab Simulink implementation.

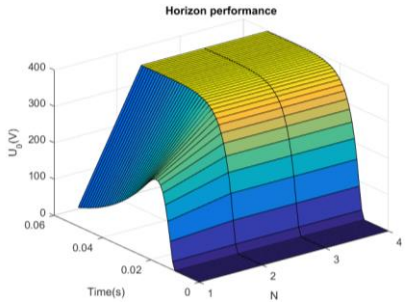

Figure 9
Step response of the system as a function of the horizon length (*N*)

5.3 Simulation Results

The simulation results are produced with Matlab/Simulik. The discrete model's (9) simulation frequency was $f_s = 10^6 Hz$, with the model parameters represented in Table 3, and with the control structure shown on Fig. 4. The EMPC performance is shown in Fig. 10 and Fig. 11.

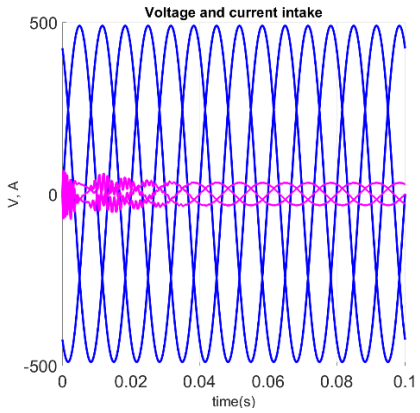

Figure 10
Three-phase voltage and current intake of the CSR with EMPC

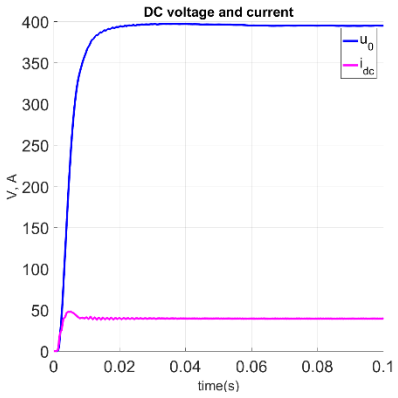

Figure 11
Resulting current and voltage trajectories of the CSR with (EMPC)

More details about the Matlab simulation are presented in [34].

5.4 Comparison with a State Feedback Control

On the DC side, not only the output voltage u_0 but also the inductor current i_{dc} needs to be controlled. Described in [28], a state feedback control with optimal parameters can be used as a reference based on the model properties listed in Table 3, with output voltage u_0 and DC bus current i_{dc} chosen as the state

variables. Since u_0 is a DC quantity in steady state, an integrator signal is introduced to diminish the steady-state error. The structure of the controller is represented in Fig. 12.

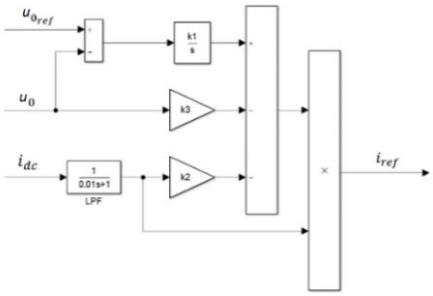

Figure 12
Simple DC side state feedback control structure

The tuning constants applied and calculated according to [24] are:

$$k1 = \frac{\omega_n^3}{1.5U_n\omega_{dc}^2},\ k2 = \frac{1.9\omega_n L_{dc}}{1.5U_n},\ k3 = \frac{2.2\omega_n^2}{1.5U_n(\omega_{dc}^2-1)}, \tag{26}$$

where $\omega_n = 1.1, \omega_{ac} = \frac{1}{\sqrt{L_{ac}C_{ac}}}$, and $\omega_{dc} = \frac{1}{\sqrt{L_{dc}C_{dc}}}$.

The state feedback controllers block on the diagram is taking the controller's place, shown on Fig. 2. The independent outputs are the high pass filter's output $i_{rHF(d)}$ and the controller's output $i_{rcontrol(d)}$. The sum of the independent current values is converted to Clarke frame to be able to govern the switching states of the IGBT's. This can be done because $i_{rHF(d)}$ has only high frequency components and $i_{rcontrol(d)}$ has low frequency components due to the differences in LC time constants, as discussed in the second section. Then, the control signal governing the switches is applied in the same manner, described at the start of Section 3. The state feedback control's performance in comparison with the EMPC is shown in Fig. 13.

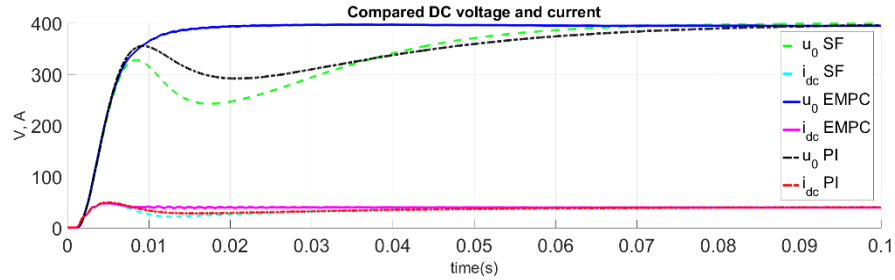

Figure 13
Resulting current and voltage trajectories of the CSR with explicit model predictive control (MPC) compared state feedback control (SF), and simple proportional-integral control (PI), where $P = 0.01$, and $I = 100$, with the respect of constraints described in (19)

Appendix

Table 3
The applied parameters in model and controller design

Parameter	Value	Description
R	0.3 Ω	Phase resistance
R_{load}	10 Ω	Load resistance
L_{ac}	1 mH	AC-side filter inductance
L_{dc}	30 mH	Choke inductance
C_{ac}	30 μF	AC-side filter capacitance
C_{dc}	400 μF	DC-side capacitance
f_s	$10^{-6} Hz$	Simulation frequency
f	50 Hz	Network frequency
f_{pwm}	20 kHz	Modulation frequency
U_n	400 V	Network line voltage
R_w	$\boldsymbol{I}_2$	State weighting matrix
Q_w	$10^{-6}\boldsymbol{I}_2$	Input weighting matrix
$\boldsymbol{N}$	2	Control horizon
$\boldsymbol{\omega}_{\mathrm{n}}$	1.1	undamped oscillation frequency

Conclusions

The constrained, model-based optimal control of a current source rectifier has been presented in this paper. The dynamic model of a three-phase current source rectifier has been developed in Park frame. The proposed model has been examined from the design and implementation points of view with the purpose of explicit model-based predictive control. It proved to be the case that the regular set of differential equations of the CSR appears to be too complex, and contains non-linearity for such a design approach. To address this issue the usage of separated AC and DC equation sets was suggested to avoid linearization and complexity reduction. This solution eliminates bilinearity and enables the application of linear control design techniques. Current-based SVPWM of the three-phase converter has been used with an emphasis on the reduction of switching losses. Throughout the article the explicit model predictive control method is described and the method's effectiveness compared to conventional state feedback control is show. The implementation and simulation experiments have been performed in Matlab/Simulink environment. Moreover, the proper implementation of the system in a modern DSP chip will result in real-time operation.

Acknowledgement

Attila Fodor acknowledges the financial support of Széchenyi 2020 under the EFOP-3.6.1-16-2016-00015. Attila Magyar was supported by the János Bolyai Research Scholarship of the Hungarian Academy of Sciences.

References

[1] I. Vajda. Y. N. Dementyev, K. N. Negodin, N. V. Kojain, L. S. Udut, Irina. A. Chesnokova: Limiting Static and Dynamic Characteristics of an Induction Motor under Frequency Vector Control, Acta Polytechnica Hungarica, Vol. 14, No. 6, 2017

[2] B. Ghalem, B. Azeddine: Six-Phase Matrix Converter Fed Double Star Induction Motor, Acta Polytechnica Hungarica, Vol. 7, No. 3, 2010

[3] S. Gupta, R. K. Tripathi: Two-Area Power System Stability Improvement using a Robust Controller-based CSC-STATCOM, Acta Polytechnica Hungarica, Vol. 11, No. 7, 2014

[4] Y. Li, P. Li, Y. Chen, D. Zhang: Single-stage three-phase current-source rectifier for photovoltaic gridconnected system, Conference of Power Electronics and Applications (EPE'14-ECCE Europe), Finland, 2014

[5] B. Exposto, R. Rodrigues, J. G. Pinto, V. Monteiro, D. Pedrosa, J. L. Afonso: Predictive Control of a Current-Source Rectifier for Solar Photovoltaic Grid Interface, Compatibility and Power Electronics (CPE) Conference, Portugal, 2015

[6] M. Chebre, A. Meroufel, Y. Bendaha: Speed Control of Induction Motor Using Genetic Algorithm-based PI Controller, Acta Polytechnica Hungarica Vol. 8, No. 6, 2011

[7] R. Salloum: Robust PID Controller Design for a Real Electromechanical Actuator, Acta Polytechnica Hungarica, Vol. 11, No. 5, 2014

[8] L. Neukirchner, P. Görbe, A. Magyar: Voltage unbalance reduction in the domestic distribution area using asymmetric inverters, Journal of Cleaner Production Vol. 142, Part 4, 20 January 2017, pp. 1710-1720

[9] F. Tahri, A. Tahri, A. Allali and S. Flazi: The Digital Self-Tuning Control of Step a Down DC-DC Converter, Acta Polytechnica Hungarica, Vol. 9, No. 6, 2012

[10] H. Gao, D. Xu, B. Wu, N. R. Zargari: Model Predictive Control for Five-level Current Source Converter with DC Current Balancing Capability, Industrial Electronics Society , IECON 2017 - 43rd Annual Conference of the IEEE, China, 2017

[11] Y. Han, L. Xu, M. M. Khan, C. Chen: Control Strategies, Robustness Analysis, Digital Simulation and Practical Implementation for a Hybrid APF with a Resonant Ac-link, Acta Polytechnica Hungarica, Vol. 7, No. 5, 2010

[12] T. Venkatraman, S. Periasamy: Multilevel Rectifier Topology with Modified Pulse Width Modulation and Reduced Switch Count, Acta Polytechnica Hungarica, Vol. 15, No. 2, 2018

[13] H. Feroura, F. Krim, B. Tabli, A. Laib: Finite-Set Model Predictive Voltage Control for Islanded Three Phase Current Source Rectifier, Conference of Electrical Engineering - Boumerdes (ICEE-B) Algeria, 2017

[14] Z. Yan, X. Xu, Z. Yang, X. Wu: Study of Effective Vector Synthesis Sequence for Three-Phase Current Rectifier, Fifth International Conference on Instrumentation and Measurement, Computer, Communication and Control (IMCCC) IEEE, 2015, pp. 1065-1070

[15] A. Ürmös, Z. Farkas, M. Farkas, T. Sándor, L. T. Kóczy, Á. Nemecsics: Application of self-organizing maps for technological support of droplet epitaxy, Acta Polytechnica Hungarica, Vol. 14, No. 4, 2017, pp. 207-224

[16] A. Chatterjee, R. Chatterjee, F. Matsuno, T. Endo: Augmented stable fuzzy control for flexible robotic arm using LMI approach and neuro-fuzzy state space modeling, IEEE Transactions on Industrial Electronics, Vol. 55, No. 3, 2008, pp. 1256-1270

[17] T. Haidegger, L. Kovács, R. Precup, B. Benyó, Z. Benyó, S. Preitl: Simulation and control for telerobots in space medicine, Acta Astronautica, Vol. 181, No. 1, 2012, pp. 390-402

[18] S. Vrkalovic, E. Lunca, I. Borlea: Model-free sliding mode and fuzzy controllers for reverse osmosis desalination plants, International Journal of Artificial Intelligence, Vol. 16, No. 2, 2018, pp. 208-222

[19] C. B. Regaya, A. Zaafouri, A. Chaari: A New Sliding Mode Speed Observer of Electric Motor Drive Based on Fuzzy-Logic, Acta Polytechnica Hungarica, Vol. 11, No. 3, 2014

[20] K. Széll, P. Korondi: Mathematical Basis of Sliding Mode Control of an Uninterruptible Power Supply, Acta Polytechnica Hungarica, Vol. 11, No. 3, 2014

[21] A. Kelemen, N. Kutasi, M. Imecs, I. I.I ncze: Constrained Optimal Direct Power Control of Voltage-Source PWM Rectifiers, International Conference on Intelligent Engineering Systems (INES) IEEE International Conference, Las Palmas of Gran Canaria, Spain, 2010

[22] A. Tahri, H. M. Boulouiha, A. Allali and T. Fatima: Model Predictive Controller-based, Single Phase Pulse Width Modulation (PWM) Rectifier for UPS Systems, Acta Polytechnica Hungarica, Vol. 10, No. 4, 2013

[23] M. Rivera, S. Kouro, J. Rodriguez, B. Wu, V. Yaramasu, J. Espinoza and P. Melin: Predictive Current Control in a Current Source Rectifier Operating with Low Switching Frequency, 4th International Conference on Power Engineering, Energy and Electric Drives, Turkey, 2013

[24] A. Godlewska, A. Sikorski: Predictive control of current source rectifier, Selected Problems of Electrical Engineering and Electronics (WZEE), IEEE, 2015, pp. 1-6

[25] N. Muthukumar, S. Srinivasan, K. Ramkumar, K. Kannan, V. E. Balas: Adaptive Model Predictive Controller for Web Transport Systems, Acta Polytechnica Hungarica, Vol. 13, No. 3, 2016

[26] N. Kutasi, A. Kelemen, M. Imecs: Constrained Optimal Control Of Three-Phase AC-DC Boost Converters, Automation Quality and Testing Robotics (AQTR) IEEE International Conference, Cluj-Napoca, Romania, 2010

[27] S. F. Ahmed, Ch. F. Azim, H. Desa, A. T. Hussain: Model Predictive Controller-based, Single Phase Pulse Width Modulation (PWM) Rectifier for UPS Systems, Acta Polytechnica Hungarica, Vol. 11, No. 6, 2014

[28] Y. Zhang, Y. Yi, P. Dong, F. Liu, Yong Kang: Simplified Model and Control Strategy of Three-Phase PWM Current Source Rectifiers for DC Voltage Power Supply Applications, IEEE Journal of emerging and selected topics in power electronics, Vol. 3, No. 4, december 2015

[29] A. Bemporad, M. Morari, V. Dua, Efstratios N. Pistikopoulos: The explicit linear quadratic regulator for constrained systems. Automatica Vol. 38, 2002, pp. 3-20

[30] M. Herceg, M. Kvasnica, C. N. Jones, M. Morari: Multi-Parametric Toolbox 3.0, Proceedings of the European Control Conference, Zürich, Switzerland, 2013, pp. 502-510

[31] N. Kutasi, A. Kelemen, Sz. Matyasi, M. Imecs: Hardware implementation of explicit mode-predictive control of three phase PWM rectifiers, ICCC2010 Eger, Hungary, 2010, pp. 133-136

[32] L. Moussaoui, A. Moussi: An open loop space vector PWM control for CSR-fed field oriented induction motor drive with improved performances and reduced pulsating torque, Proceedings of the 6th WSEAS international conference on Automation & information, March 2005, Part 4. pp. 329-335

[33] M. Kvasnica, I. Rauová and M. Fikar: Automatic code generation for real-time implementation of Model Predictive Control, 2010 IEEE International Symposium on Computer-Aided Control System Design, Yokohama, 2010, pp. 993-998

[34] L. Neukirchner: Constrained Predictive Control of Three-Phase BuckRectifiers Simulation details, http://virt.uni-pannon.hu/ver/index.php/en/projects/30-empc-csr, 2019